Lecture 6

LCAO tight binding hamiltonian

The starting point of this model is the decomposition of the total single-electron Hamiltonian into:

$$H = Hat + \Delta U(r) \ ,$$

where Hat contains the kinetic energy plus the potential of a single ion (the one placed at R=0, say), and $\Delta U(r)$ is the potential generated by all the others ions in the lattice except the one already considered. The eigenfunctions of the atomic problem satisfy the Schrödinger equation

$$H\,\varphi n(r) = En\,\varphi n(r) \ ,$$

where n represents collectively a full set of (orbital) atomic quantum numbers.

We then expand a generic state localized around the atom as

$$\varphi(r) = \sum n\ b_n\ \varphi_n(r)$$

[notice that this basis set is not complete as the continuum states of the atom are left out of the sum].

We than make a combination of such localized states, with the symmetry of the lattice:

$$\psi(r) = \sum_R e^{(i\ k\cdot R)}\ \varphi(r-R)$$

For fixed k, we plug this state into the Schrödinger equation:

$$H\,\psi(r) = [Hat + \Delta U(r)]\,\psi(r) = E(k)\,\psi(r)$$

This differential equation maps to a matrix equation by multiplication on the left by $\varphi_m^*(r)$ and integration over the r variable:

$$\sum_n A(k)_{mn}\, b_n = E(k) \sum_n S(k)_{mn}\, b_n$$

This, for each fixed k, is a generalized eigenvalue problem for the matrix A(k), with a "metric" matrix B in place of the identity. E(k) represents the eigenvalue, corresponding to the eigenvector b (of course, also b is k-dependent, in general). The Hamiltonian matrix above is:

$$A(k)_{mn} = \sum_R e^{(i\,k\cdot R)} \int \varphi_m^*(r)\, H\, \varphi_n(r-R)\, dr$$

The Overlap matrix above is:

$$S(k)_{mn} = \sum_R e^{(i\,k\cdot R)} \int \varphi_m^*(r)\, \varphi_n(r-R)\, dr$$

where the sums over R extend over all the lattice points.

This is conveniently rearranged (using the decomposition H = Hat + ΔU(r), the fact that φm*(r) are eigenstates of H_{at} and the orthonormality of φn(r) and φm(r)) into:

$$\sum_n C(k)_{mn}\, b_m = (E(k) - E_m) \sum_n S(k)_{mn}\, b_n$$

where the new matrix C(k) contains what is left of the Hamiltonian, i.e.

$$C(k)_{mn} = \sum_R e^{(i\, k\cdot R)} \int \varphi m^*(r)\, \Delta U(r)\, \varphi n(r-R)\, dr$$

Now the eigenvalue (E(k) - Em) of the generalized secular problem measures the displacement of the "band" energy E(k) with respect to the original atomic value E_m.

The size of this matrix eigenvalue problem is clearly as large as the number of eigenstates of the atomic problem, i.e. infinite. It is therefore necessary to do some approximation here. In particular, one could hope that all the off-diagonal matrix elements of the matrices at the right side of this eq. could be neglected for some given level m. This cannot work for atomic degenerate levels where the couplings between the degenerate levels form the main part of the Hamiltonian, the one that resolves the degeneracy: for the case of d-degenerate levels, one has to solve at least a d-dimensional matrix problem (at each value of k).

The only case where it sometimes makes sense forgetting the interaction with all levels with $n \neq m$ is with atomic s ($l=0$) non-degenerate levels. In this approximation, the matrix equation becomes a 1×1 trivial problem, for which one takes $b_m=1$ and all the other $b_{n \neq m}=0$, and only the "m" energy equation:

$$C(k)_{mm} = (E(k) - Em)\, B(k)_{mm}$$

remains, with solution:

$$E(k) = Em + C(k)_{mm}/B(k)_{mm}$$

Now, in the infinite R-sums of the definitions of the B(k) and C(k) matrices, it is convenient to separate the contribution from R=0, the contribution from R in the first shell around the origin (first or nearest neighbors), the contribution of the second shell around the origin (second neighbors), etc. The R=0 contribution to B(k) is 1, and that to C(k) is

t is a negative quantity, reflecting the attraction that the "other" nuclei produce on the band electron, which was not there when the atom was isolated. We shall indicate the R≠0 contributions to B(k) and C(k) as

$$S(R)= \int \varphi_m^*(r)\, \varphi_m(r-R)\, dr \quad \mathbf{t(R)}= \int \varphi_m^*(r)\, \Delta U(r)\, \varphi_m(r-R)\, dr$$

respectively. Noting that by symmetry $\beta(-R)=\beta(R)$ and $\gamma(-R)=\gamma(R)$, and that in all Bravais lattices in the sums over R when some vector R is present, also -R is present, one can replace the complex exponentials with cosines, and rearrange the solution for E(k) to:

$$E(k) = Em + [\chi + \sum_{R\neq 0} \cos(k\cdot R)\, \gamma(R)] / [1 + \sum_{R\neq 0} \cos(k\cdot R)\, \beta(R)]$$

This E(k) gives the tight-binding band structure in terms of a set of parameters $\beta(R)$, χ and $\gamma(R)$. We also have an explicit recipe to compute these parameters in terms of overlap integrals at different sites.

Due to the localized shape of the atomic wave functions, both $\beta(R)$ and $\gamma(R)$ become exponentially small for large R.

It therefore makes sense to ignore all the integrals outside some R_{max}, which would bring in only negligible corrections to the band structure E(k). In particular, the simplest approximation, that gives a band structure depending on a minimal number of parameters is to neglect all the β(R)'s (so that the denominator becomes unity) and to include only the t(R) for nearest neighbor (NN). In this approximation the expression simplifies further to:

$$E(k) = E_m + \chi + \gamma \sum_{R(NN)} \cos(k \cdot R)$$

where we indicated with t the value of t(R) for nearest neighbors.

The sign of t(R) is determined by the relative signs of the tails of the wave-functions $\varphi_m(r)$ and $\varphi_m(r-R)$ in the overlapping region. For s-orbitals, t(R) has the same sign as $\Delta U(r)$, i.e. negative. As a consequence, s-band tight binding places the bottom of the band at k=0 (similarly to a free- electron-like dispersion).

However, for p bands one can see qualitatively that the overlapping tails of the wave-functions $\varphi_m(r)$ and $\varphi_m(r-R)$ can have opposite sign (the p wave-function changes sign across some plane passing in the nucleus), thus t(R)>0 in that case. As a consequence, a p band shows typically a

band maximum at k=0, with negative curvature of E(k)

From Book:
Electronic
structure
And the
properties of
Solids,
W.A. Harrison

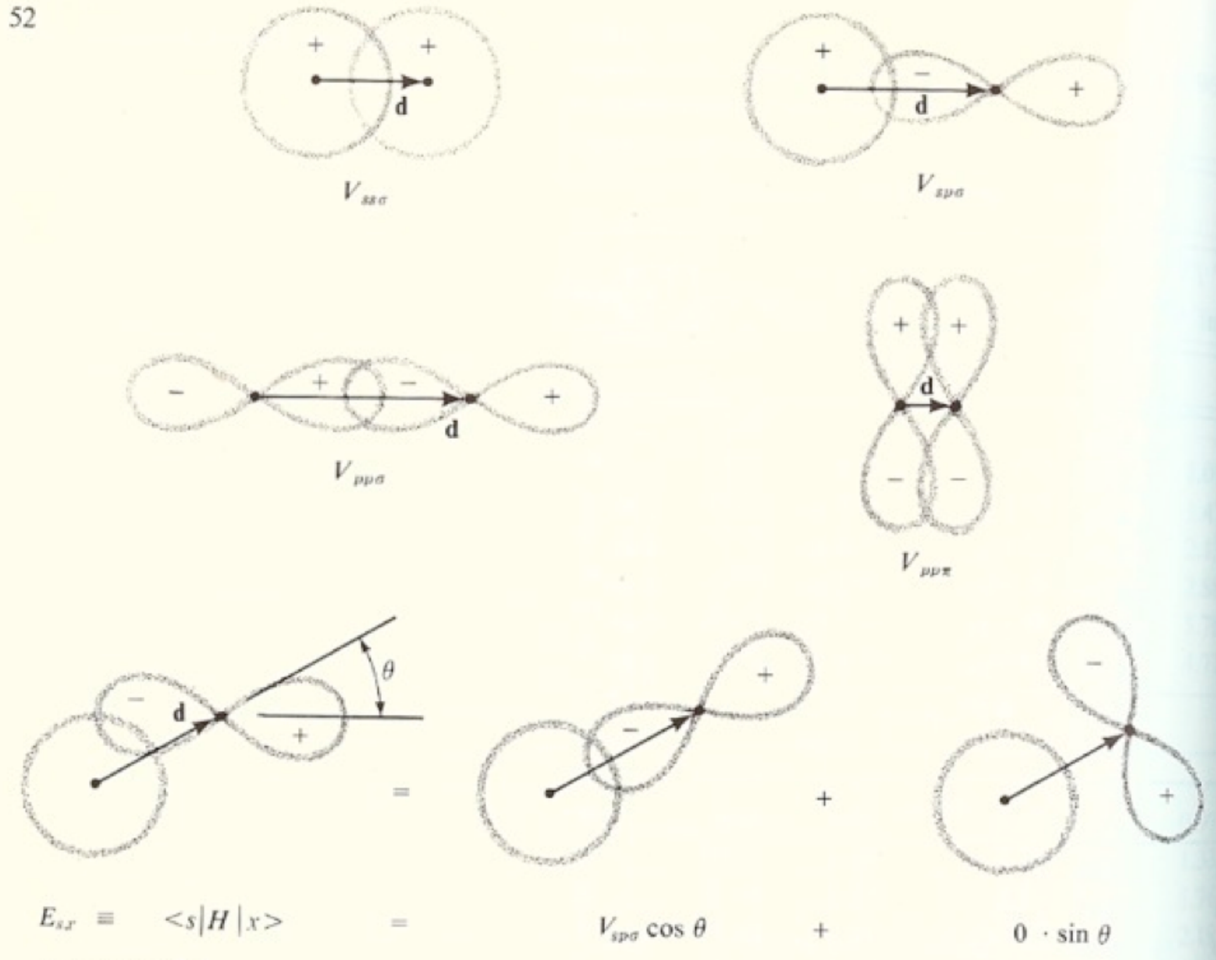

FIGURE 2-8

The four types of interatomic matrix elements entering the study of *s*- and *p*-bonded systems are chosen as for diatomic molecules as shown in Fig. 1-11. Approximate values for each are obtained from the bond length, or internuclear distance, d, by $V_{ij} = \eta_{ij}\hbar^2/md^2$, with n_{ij} taking values given in Table 2-1 and in the Solid State Table at the back of the book. When *p* orbitals are not oriented simply as shown in the upper diagrams, they may be decomposed geometrically as vectors in order to evaluate matrix elements as illustrated in the bottom diagrams. It can be seen that the interatomic matrix element at the bottom right consists of cancelling the contributions that lead to a vanishing matrix element.

From Book: Physical properties of Carbon nanotubes; Saito and Dresselhaus^2

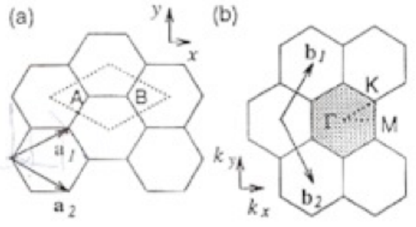

Fig. 2.3: (a) The unit cell and (b) Brillouin zone of two-dimensional graphite are shown as the dotted rhombus and the shaded hexagon, respectively. $\vec{a}_i$, and $\vec{b}_i$, $(i = 1, 2)$ are unit vectors and reciprocal lattice vectors, respectively. Energy dispersion relations are obtained along the perimeter of the dotted triangle connecting the high symmetry points, Γ, K and M.

spin orientation, both electrons occupy the bonding π energy band, which makes the total energy lower than ϵ_{2p}.

2.3 Two-Dimensional Graphite

Graphite is a three-dimensional (3D) layered hexagonal lattice of carbon atoms. A single layer of graphite, forms a two-dimensional (2D) material, called 2D graphite or a graphene layer. Even in 3D graphite, the interaction between two adjacent layers is small compared with intra-layer interactions, since the layer-layer separation of 3.35Å is much larger than nearest-neighbor distance between two carbon atoms, a_{C-C}=1.42Å. Thus the electronic structure of 2D graphite is a first approximation of that for 3D graphite.

In Fig. 2.3 we show (a) the unit cell and (b) the Brillouin zone of two-dimensional graphite as a dotted rhombus and shaded hexagon, respectively, where $\vec{a}_1$ and $\vec{a}_2$ are unit vectors in real space, and $\vec{b}_1$ and $\vec{b}_2$ are reciprocal lattice vectors. In the x, y coordinates shown in the Fig. 2.3, the real space unit vectors $\vec{a}_1$ and $\vec{a}_2$ of the hexagonal lattice are expressed as

$$\vec{a}_1 = \left(\frac{\sqrt{3}}{2}a, \frac{a}{2}\right), \quad \vec{a}_2 = \left(\frac{\sqrt{3}}{2}a, -\frac{a}{2}\right), \tag{2.22}$$

where $a = |\vec{a}_1| = |\vec{a}_2| = 1.42 \times \sqrt{3} = 2.46$Å is the lattice constant of two-dimensional graphite. Correspondingly the unit vectors $\vec{b}_1$ and $\vec{b}_2$ of the reciprocal lattice are given by:

$$\vec{b}_1 = \left(\frac{2\pi}{\sqrt{3}a}, \frac{2\pi}{a}\right), \quad \vec{b}_2 = \left(\frac{2\pi}{\sqrt{3}a}, -\frac{2\pi}{a}\right) \tag{2.23}$$

corresponding to a lattice constant of $4\pi/\sqrt{3}a$ in reciprocal space. The direction of the unit vectors $\vec{b}_1$ and $\vec{b}_2$ of the reciprocal hexagonal lattice are rotated by 90° from the unit vectors $\vec{a}_1$ and $\vec{a}_2$ of the hexagonal lattice in real space, as shown in Fig. 2.3. By selecting the first Brillouin zone as the shaded hexagon shown in Fig. 2.3(b), the highest symmetry is obtained for the Brillouin zone of 2D graphite. Here we define the three high symmetry points, Γ, K and M as the center, the corner, and the center of the edge, respectively. The energy dispersion relations are calculated for the triangle ΓMK shown by the dotted lines in Fig. 2.3(b).

As discussed in Sect. 2.3.2, three σ bonds for 2D graphite hybridize in a sp^2 configuration, while, and the other $2p_z$ orbital, which is perpendicular to the graphene plane, makes π covalent bonds. In Sect. 2.3.1 we consider only π energy bands for 2D graphite, because we know that the π energy bands are covalent and are the most important for determining the solid state properties of graphite.

2.3.1 π Bands of Two-Dimensional Graphite

Two Bloch functions, constructed from atomic orbitals for the two inequivalent carbon atoms at A and B in Fig. 2.3, provide the basis functions for 2D graphite. When we consider only nearest-neighbor interactions, then there is only an integration over a single atom in $\mathcal{H}_{AA}$ and $\mathcal{H}_{BB}$, as is shown in Eq. (2.16), and thus $\mathcal{H}_{AA} = \mathcal{H}_{BB} = \epsilon_{2p}$. For the off-diagonal matrix element $\mathcal{H}_{AB}$, we must consider the three nearest-neighbor B atoms relative to an A atom, which are denoted by the vectors $\vec{R}_1, \vec{R}_2$, and $\vec{R}_3$. We then consider the contribution to Eq. (2.17) from $\vec{R}_1, \vec{R}_2$, and $\vec{R}_3$ as follows:

$$\begin{aligned} \mathcal{H}_{AB} &= t(e^{i\vec{k}\cdot\vec{R}_1} + e^{i\vec{k}\cdot\vec{R}_2} + e^{i\vec{k}\cdot\vec{R}_3}) \\ &= tf(k) \end{aligned} \tag{2.24}$$

where t is given by Eq. (2.18)* and $f(k)$ is a function of the sum of the phase factors of $e^{i\vec{k}\cdot\vec{R}_j}$ $(j = 1, \cdots, 3)$. Using the x, y coordinates of Fig. 2.3(a), $f(k)$ is given by:

$$f(k) = e^{ik_x a/\sqrt{3}} + 2e^{-ik_x a/2\sqrt{3}} \cos\left(\frac{k_y a}{2}\right). \tag{2.25}$$

Since $f(k)$ is a complex function, and the Hamiltonian forms a Hermitian matrix, we write $\mathcal{H}_{BA} = \mathcal{H}^*_{AB}$ in which * denotes the complex conjugate. Using Eq. (2.25), the overlap integral matrix is given by $\mathcal{S}_{AA} = \mathcal{S}_{BB} = 1$, and $\mathcal{S}_{AB} = sf(k) = \mathcal{S}^*_{BA}$. Here s has the same definition as in Eq. (2.19), so that the explicit forms for $\mathcal{H}$ and $\mathcal{S}$ can be written as:

$$\mathcal{H} = \begin{pmatrix} \epsilon_{2p} & tf(k) \\ tf(k)^* & \epsilon_{2p} \end{pmatrix}, \quad \mathcal{S} = \begin{pmatrix} 1 & sf(k) \\ sf(k)^* & 1 \end{pmatrix}. \tag{2.26}$$

Solving the secular equation $\det(\mathcal{H} - E\mathcal{S}) = 0$ and using $\mathcal{H}$ and $\mathcal{S}$ as given in Eq. (2.26), the eigenvalues $E(\vec{k})$ are obtained as a function $w(\vec{k})$, k_x and k_y:

$$E_{g2D}(\vec{k}) = \frac{\epsilon_{2p} \pm tw(\vec{k})}{1 \pm sw(\vec{k})}, \tag{2.27}$$

where the + signs in the numerator and denominator go together giving the bonding π energy band, and likewise for the − signs, which give the anti-bonding π^* band, while the function $w(\vec{k})$ is given by:

$$w(\vec{k}) = \sqrt{|f(\vec{k})|^2} = \sqrt{1 + 4\cos\frac{\sqrt{3}k_x a}{2}\cos\frac{k_y a}{2} + 4\cos^2\frac{k_y a}{2}}. \tag{2.28}$$

In Fig. 2.4, the energy dispersion relations of two-dimensional graphite are shown throughout the Brillouin zone and the inset shows the energy dispersion relations along the high symmetry axes along the perimeter of the triangle shown in Fig. 2.3(b). Here we use the parameters $\epsilon_{2p} = 0$, $t = -3.033$eV, and $s = 0.129$ in order to reproduce the first principles calculation of the graphite energy bands [9, 48]. The upper half of the energy dispersion curves describes the π^*-energy anti-bonding band, and the lower half is the π-energy bonding band. The upper π^* band and the lower π band are degenerate at the K points through which

*We often use the symbol γ_0 for the nearest neighbor transfer integral. γ_0 is defined by a positive value.

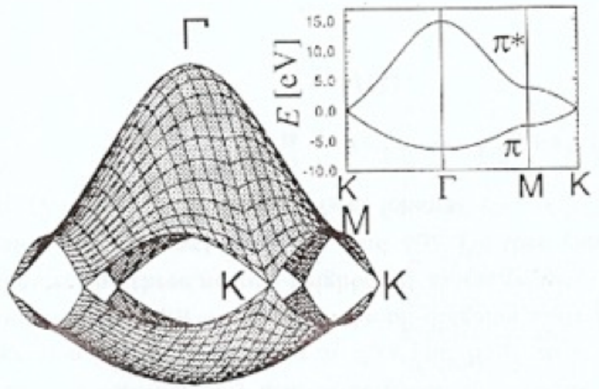

Fig. 2.4: The energy dispersion relations for 2D graphite are shown throughout the whole region of the Brillouin zone. The inset shows the energy dispersion along the high symmetry directions of the triangle ΓMK shown in Fig. 2.3(b) (see text).

the Fermi energy passes. Since there are two π electrons per unit cell, these two π electrons fully occupy the lower π band. Since a detailed calculation of the density of states shows that the density of states at the Fermi level is zero, two-dimensional graphite is a zero-gap semiconductor. The existence of a zero gap at the K points comes from the symmetry requirement that the two carbon sites A and B in the hexagonal lattice are equivalent to each other.† The existence of a zero gap at the K points gives rise to quantum effects in the electronic structure of carbon nanotubes, as shown in Chapter 3.

When the overlap integral s becomes zero, the π and π^* bands become symmetrical around $E = \epsilon_{2p}$ which can be understood from Eq. (2.27). The energy dispersion relations in the case of $s = 0$ (i.e., in the Slater–Koster scheme) are commonly used as a simple approximation for the electronic structure of a graphene layer:

$$E_{g2D}(k_x, k_y) = \pm t\left\{1 + 4\cos\left(\frac{\sqrt{3}k_x a}{2}\right)\cos\left(\frac{k_y a}{2}\right) + 4\cos^2\left(\frac{k_y a}{2}\right)\right\}^{1/2}. \tag{2.29}$$

†If the A and B sites had different atoms such as B and N, the site energy ϵ_{2p} would be different for B and N, and therefore the calculated energy dispersion would show an energy gap between the π and π^* bands.

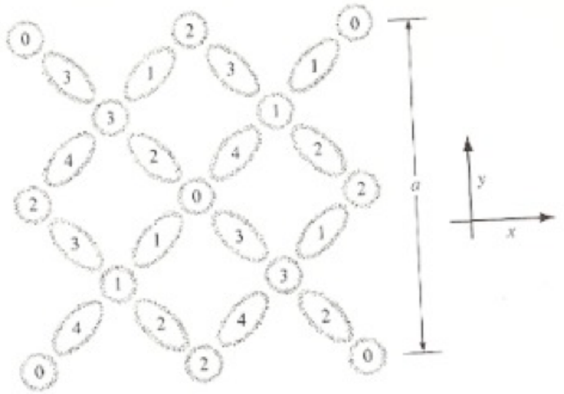

FIGURE 3-5
The numbers within the ovals represent the numbering of bond orbitals in a zincblende lattice. The small circles represent atoms; the numbers within them represent the distance below the plane of the figure in units of $a/4$.

previous section, following a procedure similar to that used for CsCl in Chapter 2. There we had a particularly simple system of identical orbitals (initially chlorine s orbitals) on a simple cubic lattice; each orbital was separated from every other by integral multiples of lattice vectors of length a in the directions of cube edges. In that case the correct linear combination of orbitals could be written immediately as $N_p^{-1/2}\Sigma_i e^{i\mathbf{k}\cdot\mathbf{r}_i}|s_i\rangle$, where $\mathbf{k}$ is the wave number characterizing the state and $|s_i\rangle$ is the atomic orbital at the site $\mathbf{r}_i$. Now we have four distinct types of bond orbitals, as indicated in Fig. 3-5 and in analogy with the three different types of p orbitals in CsCl. We also have four distinct types of antibonding orbitals. In constructing a band state as a linear combination of the eight different kinds of basis orbitals, it remains true that the coefficients for any two orbitals of the same type are related by a factor $e^{i\mathbf{k}\cdot(\mathbf{r}_i-\mathbf{r}_j)}$, where $\mathbf{k}$ is again characteristic of the state and $\mathbf{r}_i$ and $\mathbf{r}_j$ are the sites of the two orbitals. (This can be shown by using group theory and the translational symmetry of the lattice.) Symmetry alone does not determine relative values of coefficients for the eight different orbital types. However, knowledge of the translational symmetry can reduce the size of the Hamiltonian matrix shown schematically in Fig. 3-4 from 10^{23} by 10^{23} to 8 by 8, and that is the difference between an insoluble and a soluble problem.

A wave number must again be associated with every state; for each wave number we construct eight different ***Bloch sums***, four for the bond orbital types,

$$|\chi_a(\mathbf{k})\rangle = \sum_i e^{i\mathbf{k}\cdot\mathbf{r}_i}|b_a(\mathbf{r}-\mathbf{r}_i)\rangle/\sqrt{N_p}, \tag{3-19}$$

and four for the antibonding orbital types. The value N_p is the number of atom pairs, equal to the number of bonds of each type. The position $\mathbf{r}_i$ is taken to be the midpoint of the corresponding bond. Each eigenstate of wave number $\mathbf{k}$ can be

written as a linear combination of the eight Bloch sums for that wave number:

$$|\psi_\mathbf{k}\rangle = \sum_a u_a|\chi_a(\mathbf{k})\rangle. \tag{3-20}$$

In contrast, in CsCl we sufficiently simplified the matrix elements that we were able to use single Bloch sums, of the kind in Eq. (3-19), as eigenstates; we cannot do that here.

As in CsCl, the wave number is restricted so that it lies in a Brillouin Zone, but the shape of that zone is different for a zincblende or face-centered cubic crystal structure. Equivalent bond orbitals are separated by ***primitive translations*** of $[011]a/2$, $[101]a/2$, $[110]a/2$, or integral multiples of primitive translations. (This crystallographic notation was defined in Section 3-A.) Thus the addition of ***primitive lattice wave numbers*** $[111]2\pi/a$, $[1\bar{1}1]2\pi/a$, $[\bar{1}11]2\pi/a$, or integral multiples of them, to the $\mathbf{k}$ appearing in Eq. (3-19), multiplies the entire sum by the same phase factor. (This is easily verified.) This is not an independent Bloch sum; the corresponding wave numbers are said to be *equivalent*, and we need not consider any wave number that has an equivalent wave number of smaller magnitude. The Brillouin Zone shown in Fig. 3-6 is that of a zincblende lattice (or that of a face-centered cubic lattice), and is the one we shall be using. A full treatment of the topology of wave number space for this system is not possible in a single paragraph. The reader who is not familiar with this topology will find fuller accounts in any solid state physics text, such as Kittel (1976).

For any wave number in the Brillouin Zone we seek the lowest energy solution by minimizing $\langle\psi_\mathbf{k}|H|\psi_\mathbf{k}\rangle/\langle\psi_\mathbf{k}|\psi_\mathbf{k}\rangle$ with respect to u_i, in direct analogy to the minimization of energy for the system based upon two basis states, as taken up in

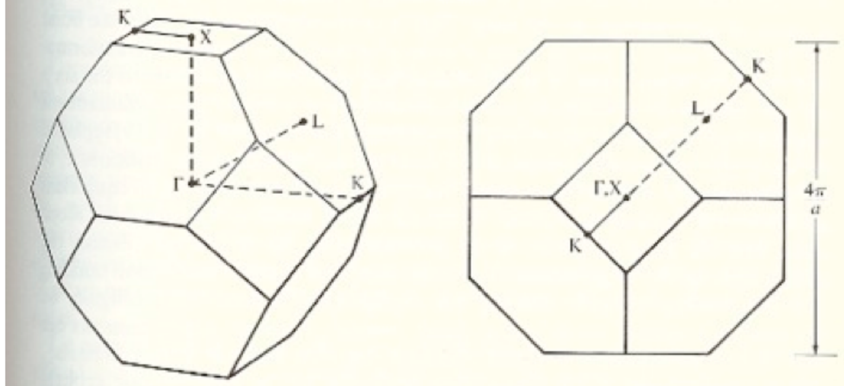

FIGURE 3-6
The Brillouin Zone and symmetry points for the zincblende (diamond, or face-centered cubic) lattice. The view at the right is along a [110] axis; that at the left has been tilted.

Chapter 1. The equations analogous to Eq. (1-10) are

$$\sum_{\beta} H_{\alpha\beta}(\mathbf{k})u_{\beta} = E_{\mathbf{k}}u_{\alpha}, \tag{3-21}$$

where the matrix elements and eigenvalues depend upon $\mathbf{k}$; that is,

$$H_{\alpha\beta} = \langle \chi_{\alpha}(\mathbf{k}) | H | \chi_{\beta}(\mathbf{k}) \rangle. \tag{3-22}$$

The eight solutions to Eqs. (3-21) are called the ***eigenstates*** of the matrix $H_{\alpha\beta}$ and are the electron states in the approximation that each eigenstate can be written in the form of Eq. (3-20).

A Return to Atomic Orbitals

At this stage we must evaluate the matrix elements and then solve Eqs. (3-21) to obtain eigenstates and energy bands. However, for our method of determining interbond matrix elements from the interatomic matrix elements of Table 2-1, the use of bonding orbitals and antibonding orbitals becomes inconvenient. For example, in Fig. 3-5, notice that we seek matrix elements between Bloch sums based upon bond orbitals of type 1 and type 2. We may focus on a particular bond orbital of type 2 and see that there are matrix elements between it and bond orbitals in adjacent bonds, and also matrix elements between it and bond orbitals in second-neighbor bonds arising from hybrids on the two atoms between, which are nearest-neighbor atoms. Thus we lose the simplicity provided by nearest-neighbor matrix elements because of our choice of basis. This will nevertheless be convenient in Chapter 7 when we seek approximate solutions. For now, we seek an exact solution, and for this it is much better to follow Chadi and Cohen (1975) in using atomic orbitals as the basis. This is obviously equivalent since the bond orbitals have been written as sums of atomic orbitals. The result of a transformation from the eight types of bond orbitals and antibonding orbitals to the six p orbitals and two s orbitals on the two atom types is a set of eight simultaneous equations of the form of Eq. (3-21), but with the Bloch sums of Eq. (3-19) replaced by sums over equivalent atoms (sums over cations or anions) at positions $\mathbf{r}_i$ of atomic s orbitals, or sums over one of the orientations of p orbitals on equivalent atoms. It will be more convenient to obtain matrix elements between such Bloch sums, and the diagonalization of the corresponding matrix will give exactly the same bands as the diagonalization of the equivalent matrix based upon bonding and antibonding orbitals. Making this change also bypasses the ambiguity we discussed concerning covalent and polar energies, since all matrix elements can now be written explicitly in terms of matrix elements between atomic orbitals.

We redraw some of the bond orbitals of Fig. 3-5 to show atomic orbitals, orienting them along the cube directions. The set of five atoms in the upper right corner of Fig. 3-5 will suffice; the corresponding orbitals are sketched in Fig. 3-7. Imagine the central atom to be metallic.

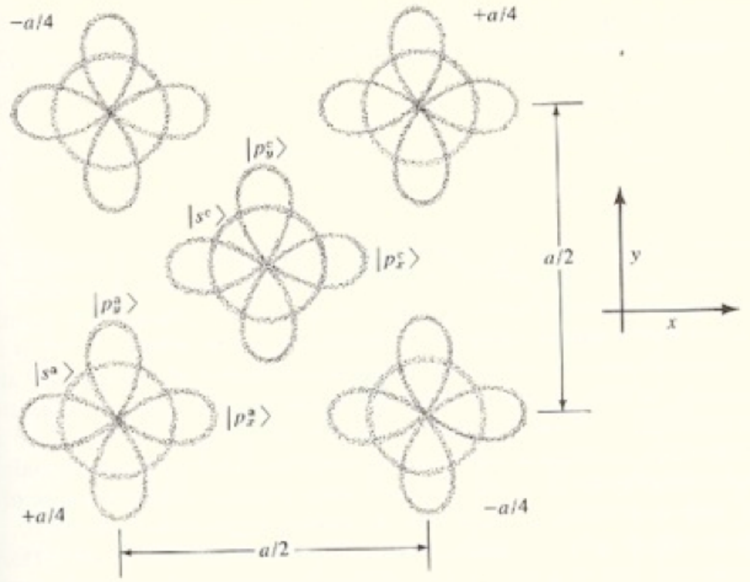

FIGURE 3-7
Numbering of atomic orbitals in a zincblende lattice. The central atom is imagined to be a metallic atom, a cation; then the four neighbors are anions. The central atom is imagined to be in the plane of the figure, the plane $z = 0$. The z-coordinate of each anion is indicated as $\pm a/4$. Orbitals $|p_z>$ are not shown.

The Hamiltonian Matrix

Consider first a matrix element $H_{xx}(\mathbf{k})$, from Eq. (3-22), where both Bloch sums are taken over a p orbital on the metallic atom, oriented in the x-direction. In zincblende, since all nearest neighbors are nonmetallic atoms, no nearest-neighbor matrix elements enter the calculation; the matrix element $H_{p_x^c p_x^c}(\mathbf{k})$ of Eq. (3-22) becomes simply a sum over N_p p orbitals oriented in the x-direction, divided by N_p, which is simply ε_p^c, with c denoting "cation." Similarly, every other diagonal matrix element is simply the corresponding atomic term value. Furthermore, no off-diagonal matrix elements $H_{\alpha\beta}(\mathbf{k})$ couple Bloch sums of cation states with those of other cation states, or Bloch sums of anion states with those of other anion states.

Let us now look at $H_{\alpha\beta}(\mathbf{k})$, from Eq. (3-22), where α corresponds to a cation s orbital and β to an anion s orbital. Each orbital $\langle s^c|$ in the sum making up the state $\langle \chi_{\alpha}(\mathbf{k})|$ will have matrix elements $V_{ss\sigma}$ between it and the four neighboring orbitals $|s^a\rangle$, indicated in Fig. 3-7; each of these neighboring orbitals enters the matrix element $V_{ss\sigma}$ with a phase factor differing from that of the $|s^c\rangle$ orbital by

$e^{i\mathbf{k}\cdot\mathbf{d}_i}$, with $\mathbf{d}_i$ being the vector distance to that neighbor. The two factors of $N_p^{-1/2}$ are cancelled by the number of terms in the χ_α sum, leading to a matrix element

$$H_{s^c s^a}(\mathbf{k}) = V_{ss\sigma}\sum_i e^{i\mathbf{k}\cdot\mathbf{d}_i}$$
$$= V_{ss\sigma}\left[e^{i(k_x+k_y+k_z)a/4} + e^{i(k_x-k_y-k_z)a/4} + e^{i(-k_x+k_y-k_z)a/4} + e^{i(-k_x-k_y+k_z)a/4}\right]. \tag{3-23}$$

The matrix element $H_{s^a s^c}(\mathbf{k})$ is easily seen to be the complex conjugate of this, and in fact $H_{\alpha\beta}(\mathbf{k}) = H_{\beta\alpha}(\mathbf{k})^*$ in general; that is, the matrix is Hermitian.

Similarly, the matrix element $H_{p_x^c s^a}(\mathbf{k})$ can be seen to consist of four terms, and each of the four terms is obtained by decomposing the orbital p_x^c into σ and π components for each one of the four neighbors; between the π component and the neighboring s orbital the matrix element is zero but between the σ component and the neighboring s orbital the matrix element is $\pm V_{sp\sigma}/3^{1/2}$. The $3^{-1/2}$ is the coefficient in the decomposition; and the sign of the matrix element depends upon whether the s orbital lies in the direction of the positive or negative lobe of the p orbital. This is sufficient to show how the matrix elements are evaluated.

We now simply give the results obtained by Chadi and Cohen (1975) for each matrix element. The neighbors to the cation (designated with subscript numerals) and their vector distances are given as

$$\left.\begin{aligned}\mathbf{d}_1 &= [111]a/4;\\ \mathbf{d}_2 &= [1\bar{1}\bar{1}]a/4;\\ \mathbf{d}_3 &= [\bar{1}1\bar{1}]a/4;\\ \mathbf{d}_4 &= [\bar{1}\bar{1}1]a/4.\end{aligned}\right\} \tag{3-24}$$

Then four sums of phase factors are defined by

$$\left.\begin{aligned}g_0(\mathbf{k}) &= e^{i\mathbf{k}\cdot\mathbf{d}_1} + e^{i\mathbf{k}\cdot\mathbf{d}_2} + e^{i\mathbf{k}\cdot\mathbf{d}_3} + e^{i\mathbf{k}\cdot\mathbf{d}_4};\\ g_1(\mathbf{k}) &= e^{i\mathbf{k}\cdot\mathbf{d}_1} + e^{i\mathbf{k}\cdot\mathbf{d}_2} - e^{i\mathbf{k}\cdot\mathbf{d}_3} - e^{i\mathbf{k}\cdot\mathbf{d}_4};\\ g_2(\mathbf{k}) &= e^{i\mathbf{k}\cdot\mathbf{d}_1} - e^{i\mathbf{k}\cdot\mathbf{d}_2} + e^{i\mathbf{k}\cdot\mathbf{d}_3} - e^{i\mathbf{k}\cdot\mathbf{d}_4};\\ g_3(\mathbf{k}) &= e^{i\mathbf{k}\cdot\mathbf{d}_1} - e^{i\mathbf{k}\cdot\mathbf{d}_2} - e^{i\mathbf{k}\cdot\mathbf{d}_3} + e^{i\mathbf{k}\cdot\mathbf{d}_4}.\end{aligned}\right\} \tag{3-25}$$

Finally, composite matrix elements are defined by

$$\left.\begin{aligned}E_{ss} &= V_{ss\sigma};\\ E_{sp} &= -V_{sp\sigma}/3^{1/2};\\ E_{xx} &= 1/3V_{pp\sigma} + 2/3V_{pp\pi};\\ E_{xy} &= 1/3V_{pp\sigma} - 1/3V_{pp\pi}.\end{aligned}\right\} \tag{3-26}$$

TABLE 3-1
The LCAO Hamiltonian matrix for the zincblende structure. Parameters are defined in Eqs. (3-25) and (3-26).

	s^c	s^a	p_x^c	p_y^c	p_z^c	p_x^a	p_y^a	p_z^a
s^c	ε_s^c	$E_{ss}g_0$	0	0	0	$E_{sp}g_1$	$E_{sp}g_2$	$E_{sp}g_3$
s^a	$E_{ss}g_0^*$	ε_s^a	$-E_{sp}g_1^*$	$-E_{sp}g_2^*$	$-E_{sp}g_3^*$	0	0	0
p_x^c	0	$-E_{sp}g_1$	ε_p^c	0	0	$E_{xx}g_0$	$E_{xy}g_3$	$E_{xy}g_2$
p_y^c	0	$-E_{sp}g_2$	0	ε_p^c	0	$E_{xy}g_3$	$E_{xx}g_0$	$E_{xy}g_1$
p_z^c	0	$-E_{sp}g_3$	0	0	ε_p^c	$E_{xy}g_2$	$E_{xy}g_1$	$E_{xx}g_0$
p_x^a	$E_{sp}g_1^*$	0	$E_{xx}g_0^*$	$E_{xy}g_3^*$	$E_{xy}g_2^*$	ε_p^a	0	0
p_y^a	$E_{sp}g_2^*$	0	$E_{xy}g_3^*$	$E_{xx}g_0^*$	$E_{xy}g_1^*$	0	ε_p^a	0
p_z^a	$E_{sp}g_3^*$	0	$E_{xy}g_2^*$	$E_{xy}g_1^*$	$E_{xx}g_0^*$	0	0	ε_p^a

SOURCE: Obtained from form given by Chadi and Cohen (1975).

(In Eqs. 3-25 and 3-26 our definitions differ by a factor of four from those used by Chadi and Cohen, but the final matrix is equivalent, except that we do not distinguish two types of E_{sp}.) Now the Hamiltonian matrix can be written as in Table 3-1.

The Energy Bands

All parameters have now been specified in detail; energy bands can be obtained as a function of $\mathbf{k}$ by diagonalizing the matrix in Table 3-1 for each $\mathbf{k}$. For arbitrary wave numbers this would need to be accomplished numerically, but at special wave numbers or for wave numbers along symmetry lines in the Brillouin Zone it can be accomplished analytically. Let us diagonalize the matrix analytically for the point Γ at the center of the Brillouin Zone, $\mathbf{k} = 0$. At $\mathbf{k} = 0$, $g_1 = g_2 = g_3 = 0$ and $g_0 = 4$. Thus all off-diagonal matrix elements in Table 3-1 vanish except those coupling s^c with s^a, those coupling p_x^c and p_x^a, and so on. The

solution for each coupled pair of Bloch sums is immediate, leading to energies of

$$\left.\begin{aligned} E &= \frac{\varepsilon_s^c + \varepsilon_s^a}{2} \pm \sqrt{\left(\frac{\varepsilon_s^c - \varepsilon_s^a}{2}\right)^2 + (4E_{ss})^2}; \\ E &= \frac{\varepsilon_p^c + \varepsilon_p^a}{2} \pm \sqrt{\left(\frac{\varepsilon_p^c - \varepsilon_p^a}{2}\right)^2 + (4E_{xx})^2}. \end{aligned}\right\} \tag{3-27}$$

The energy in the second equation is triply degenerate, giving one state for p_x, one for p_y, and one for p_z orbitals. The expressions in Eqs. (3-27) will prove extremely important in the discussions that follow.

Chadi and Cohen (1975) gave expressions for the values at other symmetry points and along some symmetry lines; they are analogous in form to those at Eqs. (3-27); some are listed in Chapter 6. Chadi and Cohen then adjusted the matrix elements E_{ss}, and so on, to fit the bands of diamond, silicon, germanium, and a few compounds. (In part of their study a second-neighbor interatomic matrix element was also included; in this book that matrix element is suppressed.) The fit of their bands for silicon and germanium led to the values used in this book to determine the parameters for Table 2-1 and the Solid State Table. Thus a plot of the bands for germanium, given in Fig. 3-8,a, is in some sense a fit to the bands of germanium. Comparison with the known bands, shown in Fig. 3-8,b, indicates that at least for the lower bands the fit is very good.

At the same time, calling this a *fit* to the bands is very much understating the accomplishment. The set of four parameters in Table 2-1 and the term values in Table 2-2 (all in the Solid State Table) allow calculation of energy bands for any of the homopolar semiconductors or any of the zincblende-structure compounds, as simply for one as for the other, without computers, with consistent accuracy, and without need for a previous accurate calculation for that compound. Only in first-row compounds is there indication of significant uncertainty in the results. Furthermore, as we noted in Table 2-1, the theoretical matrix elements are very nearly equal to the ones obtained by fitting bands; thus, if we had plotted bands in Fig. 3-8,a that were based upon purely theoretical parameters, the curves would have been hardly distinguishable.

For germanium, the lowest four bands contain electrons and are the valence bands; notice that they can be counted at the point K,U where they are all nondegenerate. They are separated in energy from the conduction bands at higher energies; the minimum conduction-band energy, L_{1c} in germanium, lies higher than the peak of the valence band at Γ. In the LCAO calculation, there are twice as many bands as electrons since twice as many orbitals as electrons were included. The gap between valence and conduction bands is small compared to the valence-band width, indicating that germanium is near the metallic end of the covalent range of Fig. 2-3.

Comparison of LCAO bands and true bands indicates that indeed the valence bands are very accurately represented by simple LCAO theory. The conduction bands are not nearly so accurately given, though they are qualitatively correct.

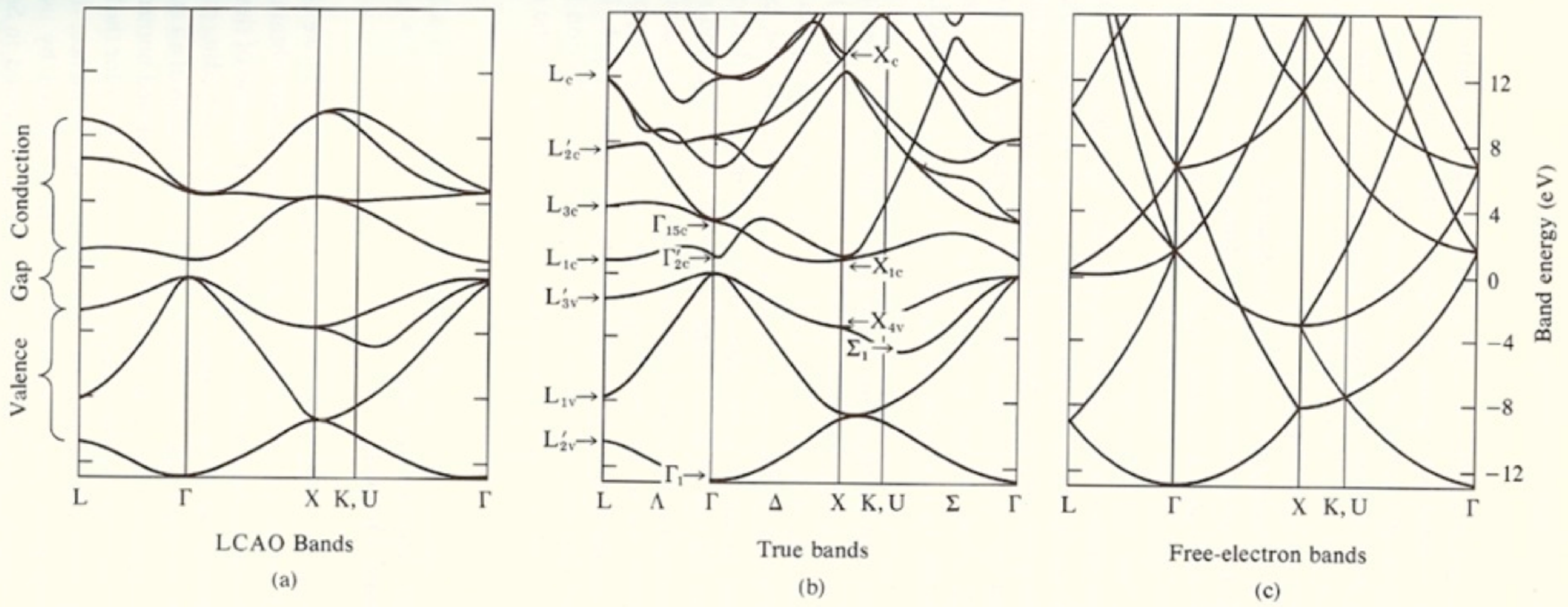

FIGURE 3-8

The energy bands of germanium. Part (a) gives the bands based upon *s* and *p* valence states and matrix elements taken from the Solid State Table. Second-neighbor interatomic matrix elements are neglected but otherwise the calculation is exact. Part (b) gives the bands obtained by Grobman, Eastman, and Freeouf (1975) by combining pseudopotential calculations with experimental optical studies; the points indicated with arrows were associated with experimental determinations. Part (c) gives the free-electron bands, $\hbar^2 k^2/(2m)$ with each state shifted into the Brillouin Zone by addition of the appropriate lattice wave number.